Simultaneous Imaging of Temperature and Soot Volume Fraction

Qing N. Chan[a,b], Paul R. Medwell[a,c], Peter A. M. Kalt[a,c], Zeyad T. Alwahabi[a,b], Bassam B. Dally[a,c], Graham J. Nathan[a,c]

[a] *Centre for Energy Technology,*
[b] *School of Chemical Engineering, and*
[c] *School of Mechanical Engineering, The University of Adelaide, S.A. 5005, AUSTRALIA*

Abstract

This paper demonstrates the first *simultaneous* single-shot imaging of temperature and soot volume fraction, measured with nonlinear regime two-line atomic fluorescence (NTLAF) and laser-induced incandescence (LII), respectively. The measurements are performed in laminar premixed and nonpremixed flames, and in a wrinkled nonpremixed flame. No significant interference of the two measurements on each other is observed. This study demonstrates a major advance in the capacity to assess the interdependence of temperature and soot in flames of practical significance.

Keywords: Temperature, Soot, Two-Line Atomic Fluorescence, Laser-Induced Incandescence, Simultaneous

1. Introduction

Soot is one of the key components in many combustion systems. Soot, when present within a flame, plays an important role in radiative heat transfer — the dominant heat transfer mode in kilns, boilers and furnaces [1, 2].

An increased presence of soot within a flame acts to increase the flame emissivity and hence the radiative heat output. This is because soot produces broadband incandescent radiation, which typically dominates over the narrow-band radiation from intermolecular processes. The presence of soot within practical combustion systems is important because it tends to increase with physical scale, owing to the accompanying increase in residence time and reduction in strain rates. Beyond a flame, unburned soot can either be emitted as an air pollutant, or as a source of "carbon black" as feedstock for manufacturing, depending on the application [3]. While combustion processes involving soot have been widely employed for many years, the processes of its formation and destruction in practical environments are beyond present capacity to understand adequately [4]. These complex processes are governed by interdependent parameters such as fuel type, mixture fraction and temperature [5]. At the same time, many of these dependencies are coupled in the presence of turbulence. Of the various coupled dependencies, soot concentration and temperature remain crucial to the understanding of soot [6].

Soot concentration distribution measurements within a flame provide valuable insights to the study of soot growth and radiant transport [7, 8]. Temperature, on the other hand, characterizes the heat transfer process and controls the chemical and physical processes within a flame [9]. Soot and temperature have an inherent coupled dependence since temperature depends on soot concentration due to heat transfer through radiation. At the same time, the temperature affects the formation and destruction of soot in flame [10]. Therefore, a detailed understanding of soot requires the knowledge of tem-

perature and vice versa. It is well-known that simultaneous measurements of multiple parameters is highly desirable to give the most useful description of a flame [11, 12]. In a turbulent environment, it is also highly desirable for the measurements to involve more than one dimension, permitting the acquisition of spatially correlated measurements and the measurements of gradient, which are useful in research and in the study of practical combustion systems [11]. It is for this reason that detailed *simultaneous planar* measurements of soot concentration and temperature within a flame environment are essential to shed light on the complex processes associated with soot.

Laser diagnostics measurements are typically suited to provide simultaneous, multi-dimensional measurements that are well resolved [13]. Their application in flames containing soot has been problematic, however [14]. Absorption, scatter, and other interferences due to the presence of soot and its precursors prevent many established laser diagnostic techniques from being applied reliably to such flames. Several approaches, such as Filtered Rayleigh scattering (FRS) [15, 16] and Coherent Anti-Stokes Raman Spectroscopy (CARS) [6, 16, 17, 18], have been explored for measurements in sooting flames. FRS is susceptible to variation in the Rayleigh cross-section across the reaction zone, further complicated by the requirement for the knowledge of the spectral broadening behaviour. These variables are difficult to account for, especially in turbulent nonpremixed imaging applications [19]. CARS, on the other hand, is limited by the necessity for line-of-sight optical access, the experimental complexity, and the lack of spatial fidelity (typically of the order of millimetres) in comparison to planar techniques [13]. However, the limitation of the CARS technique to a single point mea-

surement remains the main limitation. Alternative techniques to FRS and CARS have also been developed that may offer measurements in sooting environments [20, 21, 22], but remain immature. There is therefore a need for other methods for planar imaging of temperature in the presence of soot.

Perhaps the most promising alternative to facilitate temperature imaging in a sooting environment is Two-Line Atomic Fluorescence (TLAF), using indium as the seeded atomic species [23, 24, 25]. The inelastic nature of the TLAF technique enables optical filtering to minimize interferences from spurious scattering, allowing measurements to be performed in particle-laden environments, notably containing soot [26, 27]. TLAF offers two-dimensional imaging, with the added benefits of good sensitivity within a temperature range relevant to combustion and insensitivity to collisional quenching effects [28]. Significant breakthrough in the capabilities of TLAF to provide single-shot imaging was provided by the authors [29] who extended the technique into the nonlinear excitation regime. Nonlinear regime two-line atomic fluorescence (NTLAF) was shown to provide superior signal and reduce single-shot precision (determined by interpixel noise) in premixed flames from $\sim$250K for conventional TLAF to $\sim$100K. However, previous investigations have mostly been limited to laminar premixed environments. Also, the simultaneous application of the two methods has the potential to result in interference and it is therefore necessary to demonstrate that simultaneous imaging is possible.

For the reasons outlined above, the aim of the present paper is to assess the technical feasibility of conducting *simultaneous* single-shot temperature imaging using NTLAF and soot volume fraction measurements with the laser-

induced incandescence (LII) technique [30]. These measurement techniques are selected with a view towards future application in turbulent environments as they offer the advantage of planar imaging. The present paper also aims to measure and evaluate the fluorescence, temperature and soot volume fraction single-shot images. A laminar premixed, a laminar nonpremixed and a wrinkled nonpremixed flame are chosen to provide flame mediums with distinct features to be used for these assessments.

2. Experimental

2.1. Burner details

The burner used in this study consists of a circular ceramic honeycomb matrix (⌀80 mm) of 1 × 1 mm square pores with ∼0.25 mm wall thickness. The honeycomb matrix is encased in a brass annular tube of 80 mm ID. A second annular tube of 100 mm ID is aligned to provide co-annular flow. This burner is used for calibration and to stabilise the premixed and nonpremixed flames examined in this paper. When operated in premixed mode the flame is shrouded by a nitrogen coflow. In the nonpremixed mode no coflow was introduced. To prevent buoyancy-driven instability, a stabilisation plate (⌀100 mm) is mounted 30 mm above the burner face. The fuel used throughout this paper is industrial grade ethylene (>99.5% C_2H_4).

Indium chloride is dissolved in methanol as the source of the indium atoms for excitation using the NTLAF technique. The seeding solution is introduced into the fuel stream as an aerosol generated by a pair of capillary tube nebulisers mounted at the base of the burner. The surrounding air was not seeded with indium, as this does not improve the level of signal, and

would lead to additional impact of the solvent on the flame [31]. The mole fraction of the solvent in the inlet gases is ∼3%. In the nonpremixed mode, the majority of the air flow is turned off, leaving sufficient air to generate aerosol from the nebulisers to allow seeding of the flow. The corresponding air fuel ratio is 2.7:1 by volume, thus exhibiting the same traits as nonpremixed flames. The large cross sectional area of the burner gives a low strain rate (flame time constant, $D/U = 2.33$ s [32]), results in spatially wide flames with distinguishable features.

2.2. TLAF methodology

The TLAF excitation/detection process consists of two distinct operations [29]. Briefly, the Stokes transition requires 410 nm laser excitation, and the subsequent fluorescence is detected at 450 nm. The anti-Stokes transition uses 450 nm excitation and 410 nm detection. By adding a small time delay (∼100ns) between two excitation pulses, in conjunction with the use of 10 nm bandwidth interference filters, the Stokes fluorescence detected at 450 nm may be essentially immune from spurious scatter from the 410 nm excitation and likewise for the anti-Stokes signal. By both temporal and spectral shifting of the Stokes and anti-Stokes processes to avoid elastic scatter interferences, measurements in sooting conditions are feasible. A full description of the NTLAF theory, has been presented in a previous publication [29]. The following relationship is used to calculate flame temperature:

$$T = \frac{\Delta E_{10}/k}{ln\left(F_{21} \times (1 + \frac{C_S}{I_{20}})\right) - ln\left(F_{20} \times (1 + \frac{C_A}{I_{21}})\right) + C_T}. \quad (1)$$

Here, ΔE_{10} is the energy difference between levels, F is the fluorescence

intensity, and I is the incident laser energy. The other terms are constants. C_A and C_S are derived experimentally from the fluorescence versus irradiance plot for the two excitation schemes, whilst C_T is determined via calibration in a premixed flame as described previously [29]. Experimental calibration eliminates the need for accurate quantification of numerous experimental factors, such as laser linewidth, collection efficiency, and seed concentration [23]. It has been shown previously that the technique appears to be relatively insensitive to fuel type and flame composition, within experimental uncertainty [29, 31].

2.3. NTLAF experimental details

The experimental arrangement used in this experiment follows that described previously [29]. In brief, two Nd:YAG pumped dye lasers are tuned to 410.18 & 451.13 nm and fired with ∼100 ns separation. The two beams are combined into a co-planar sheet of ∼0.3 mm thickness. The beams are directed through a tank in the same field of view as the burner. The tank is filled with fluorescing dye to allow a shot-by-shot correction of the laser energy and profile variation across the sheet height. The frequency-shifted fluorescence from both the tank and flame is detected through interference filters using $f_{\#}1.4$ lenses onto two intensified CCD (ICCD) cameras. By appropriate image processing software, the resultant images from the two cameras are spatially matched using a three-point matching algorithm and then morphed based on the cross-correlation of a target to ensure sub-pixel spatial matching of the images. The in-plane resolution of the matched images is 380 µm.

2.4. LII experimental details

Soot volume fraction is measured using laser-induced incandescence (LII). Excitation was performed with an Nd:YAG laser (1064 nm) and collected with another ICCD camera, fitted with a 410 nm (10 nm bandwidth) interference filter. This scheme was chosen to minimise interferences [30] and is consistent with previous studies in our laboratory [33]. The LII process is delayed approximately 800 ns after the NTLAF measurements, which was found to avoid cross-talk of the LII with the NTLAF imaging. This delay is small in relation to the physical and chemical time-scales of the flame, ensuring that the NTLAF and LII measurements are virtually simultaneous. The gate-width of the LII was set to 100 ns, and the timing to be prompt with the LII excitation, as this greatly reduces the size-dependent sensitivity of the signal [34]. The LII laser sheet was 20 mm high with $\sim$0.3 mm thickness. The plateau region of the LII response curve (not shown here) occurs when the mean laser fluence exceeds $\sim$0.5 J/cm^2. The operating laser fluence was kept at $\sim$0.9 J/cm^2 throughout the experiment to ensure that the LII signals are approximately independent of the fluence variation. The wings of the sheet exhibiting lower laser fluence were clipped with a rectangular aperture. The same sheet-forming optics were used for both the NTLAF and the LII. The lenses were not achromatic, leading to a slight difference in their focal lengths. However this effect was small over the region of interest through the flame. A schematic diagram of the experimental arrangement, incorporating both the NTLAF and LII system, is shown in Fig. 1.

Following a similar methodology as Qamar *et al.* [33] calibration of the LII system was performed using laser extinction. Here, a (chopped) continuous-

wave 1064 nm laser was used to avoid absorption effects (from PAH, or similar) that may occur with the use of a 632 nm beam [35]. The soot extinction coefficient (K_e) was taken to be 9.2, as measured by Williams *et al.* [36] who found that in the infrared spectrum for in-flame soot in a co-annular ethylene flame this value did not show any significant variation with flame height. The K_e value, predicted from the Rayleigh limit expression in combination with standard literature values for the soot refractive index (e.g., Ref. [37]), was not used as there are valid concerns regarding the accuracy of this methodology [7, 36, 38].

It is noted that whilst LII is reasonably well-established, recent studies [39, 40] have revealed that primary particle size may significantly influence soot volume fraction measurements. Whilst two-colour LII is preferable, single-colour LII is capable of producing quantitative results. Through a combination of timing schemes, wavelength selection and the fluence conditions, single-colour LII is capable of achieving accurate measurements [39].

3. Results and Discussion

3.1. Laminar Premixed Flame

Figures 2(a) and 2(b) show typical single-shot indium Stokes and anti-Stokes images, which are recorded simultaneously under a spectral irradiance of approximately 1.5×10^6 W/cm^2/cm^{-1}. The images presented are 20 mm high and 50 mm wide, centred at a 10 mm height above burner (HAB). The stoichiometry of the flame presented in the figure is approximately 2.5. The SNR (ratio of the signal strength to the standard deviation of the signal in a uniform region of flame) of the Stokes and anti-Stokes images are $\sim$20:1

and ∼6:1, respectively. No image smoothing was applied in this paper to reduce inter-pixel noise, as this can degrade spatial resolution and give false information on the SNR of the images.

Applying the NTLAF theory to the fluorescence images yields the deduced temperature image in Fig. 2(c), which has an average value of ∼1300 K, and a SNR of ∼17:1 (leading to an uncertainty due to noise of ∼60 K). The temperature value is a result of the combined heat loss to the stabilisation plate, burner and to the surrounds by radiation from flame and soot.

Both the Stokes and anti-Stokes fluorescence images exhibit non-uniformity across the imaged region. This is attributed mainly to the disproportionate seeding and formation of neutral indium atoms within the flame [29, 31], as the non-uniformity of the fluorescence images is observed to follow the burner when rotated. Additionally, laser measurements indicate that extinction due to soot is approximately 5% in the present flame. This was deduced from other measurements showing that the self-absorption from indium in clean flames was negligible. Since extinction is wavelength dependent, and both Stokes and anti-Stokes excitations are similar in wavelength, the differences in the extinction affect both images approximately equally, and (within experimental uncertainty) does not affect the infered temperature measurement. Evidence of the non-uniformity of the fluorescence images having a negligible effect on the deduced temperature image is seen in Fig. 2(c). A constant temperature field is observed across the width of the burner, with no apparent temperature difference across the image. Furthermore, the path length of this flame is significantly greater than that typically encountered in nonpremixed flames and therefore the effects of the absorption (governed

by the optical thickness) are expected to be conservative relative to many future flames of interest (*viz.* turbulent nonpremixed flames).

Tuning the laser off-wavelength reveals that interferences due to soot are insignificant ($\lesssim$1%) in both Stokes and anti-Stokes images for the present flame. This demonstrates that the filtering capability of the NTLAF is adequate in suppressing soot interference.

Figure 2(d) represents the two-dimensional soot volume fraction distribution measured simultaneously with the fluorescence and temperature images shown in Fig. 2(a-c). The figure shows that the soot volume fraction of the present flame peaks at $\sim$0.07 ppm. The uniformity of the temperature field (Fig 2(c)) appears to be unaffected by the soot concentration distribution. This suggests that, for the selected flame conditions, flame temperature changes little with height above burner (HAB) despite the emergence of soot in the downstream region of the flame.

A further re-evaluation of the measured soot volume fraction based on the K_e value of 4.9, estimated from the complex refractive index of 1.57-0.56i [7, 37], gives a peak value of $\sim$0.14 ppm. It is important to note that the flames produced by the present burner are sensitive to the geometry and the placement of the plate. Therefore, it is not possible to directly compare the current measurement with previous studies. However, the observed values are similar to those of a laminar premixed ethylene-air flame with a similar arrangement, as measured by Menon *et al.* [41].

3.2. Laminar Nonpremixed Flame

Figure 3(a) and 3(b) show typical single-shot Stokes and anti-Stokes images recorded with the burner operating in nonpremixed mode. Good signal

is detected across the region of interest, namely the reaction zone. The regions without signal on either side of the reaction zone are due to a paucity of neutral indium atoms there [31].

The temperature image (Figure 3(c)) is inferred from the fluorescence images, using the calibration constants determined from the laminar premixed flame. The temperature profile exhibits a steep temperature gradient, as expected. The temperature threshold of the image is found to be 1000 K, below which the indium formation process from the indium chloride solution does not become significant [31]. Hence, those parts of images with no data are caused by temperature and/or chemical effects that are not favourable for the production of neutral indium atoms from the indium chloride.

Collected simultaneously with the temperature, the corresponding single-shot soot volume fraction distribution is presented in Fig. 3(d). The peak soot volume fraction value ($\sim$0.3 ppm) for the laminar nonpremixed flame is found to be higher than that measured for the laminar premixed flame ($\sim$0.07 ppm), which is to be expected.

Exploiting the simultaneity of the imaging measurements, Fig. 3(e) shows the overlapping nonpremixed flame temperature field and the corresponding single-shot soot distribution. A colour scale is used for the temperature and a grey shading is specified for the soot sheet to highlight different regimes within the nonpremixed flames highlighted in the figure. From Fig. 3(e) it is apparent that temperature data is available from the NTLAF at all regions when the soot is present. The soot regions are observed to be narrow and are confined to a restricted temperature range. This observation is important, especially considering that this investigation is part of a series of studies aimed

to understand the coupled dependencies between temperature and soot in flames. It shows that the NTLAF technique is well suited to such investigations. The single-shot temperature–soot distribution exhibit the qualitative features expected for a laminar nonpremixed flame [10]. The soot sheets are observed to be located at radial locations on the fuel-rich size of the peak temperature. The observation that the soot sheets are spatially separated from the high temperature regions i.e. the reaction zones is consistent with previous studies [42].

3.3. Wrinkled Nonpremixed Flame

Figure 4 presents the equivalent sets of images for a wrinkled nonpremixed case. The turbulent motions deduced from Fig. 4 were generated by removing the stabilisation plate from the burner. An external air supply was also used to physically induce a cross-flow to the flame. These figures highlight the benefits of planar imaging in providing physical insights in the study of rapidly varying two-dimensional or three-dimensional flows [43, 44].

Evident from Fig. 4(e) is that the turbulent motions result in both spatial broadening and thinning of the high temperature zones and soot sheet, relative to the profiles observed in the laminar premixed case. The soot concentration is observed to vary along the high temperature zones. Typically, increasing the strain in a laminar flame lead to a reduction in soot concentration. However, it is evident that the influence of the turbulent motions on the present flame is complex, with no simple or constant relationship between temperature and soot volume fraction. It is also interesting to note that, as in the steady case, the soot sheet does not overlap the highest temperature part of the flame. However, in the wrinkled case, the soot sheet is not found

radially inside of the highest temperature peak; rather the soot sheet abuts the high temperature sheet, but at a point of high curvature. All these observations are consistent with view that the location and the dynamics of the soot formation is closely related to the motions of the large-scale structures [42].

The influence of wrinkling in the present system on the relationship between soot volume fraction and temperature in laminar nonpremixed flames is further examined in Figure 5, which presents a scatter plot of soot volume fraction versus temperature for the present flame cases. It is clear that the flame with wrinkled structure has a much wider range of soot volume fraction values and is typically associated with lower temperatures. The details of this influence are expected to be case specific, rather than general. However, it demonstrates the need for simultaneous planar measurements to assess the relationship in detail.

4. Conclusion

The first *simultaneous* and single-shot imaging of temperature and soot volume fraction has been demonstrated using nonlinear regime two-line atomic fluorescence (NTLAF) and laser-induced incandescence (LII), respectively. The images reveal that, while NTLAF has a limited operating range, this range is sufficient to span all regions in which soot was found to be present. Furthermore, all observed features of the flame were found to be qualitatively consistent with previous work. This demonstrates the applicability of joint NTLAF–LII measurements to assess the coupled dependencies of temperature and soot in flames. The study represents a significant breakthrough in

the diagnostics capabilities in flames containing soot, which is crucial for the detailed understanding of the coupled dependence of temperature and soot in flames of practical importance.

5. Acknowledgments

The authors wish to acknowledge the support of the Centre for Energy Technology and The University of Adelaide. The Australian Research Council is also gratefully acknowledged for their funding support of this work through ARC Discovery and LIEF grant schemes.

[1] M. A. Delichatsios, J. De Ris, L. Orloff, Proc. Combust. Inst. 24 (1992) 1075–1082.

[2] J. J. Parham, G. J. Nathan, J. P. Smart, S. J. Hill, B. G. Jenkins, J. Inst. Energy 73 (2000) 25–34.

[3] Z. A. Mansurov, Combust. Explo. Shock+ 41 (2005) 727–744.

[4] I. M. Kennedy, Prog. Energy Combust. Sci. 23 (1997) 95–132.

[5] J. H. Kent, D. Honnery, Combust. Sci. Technol. 54 (1987) 383–397.

[6] K. P. Geigle, Y. Schneider-Kühnle, M. S. Tsurikov, R. Hadef, R. Lückerath, V. Krüger, W. Stricker, M. Aigner, Proc. Combust. Inst. 30 (2005) 1645–1653.

[7] M. Y. Choi, G. W. Mulhollad, A. Hamins, T. Kashiwagi, Combust. Flame 102 (1995) 161–169.

[8] N. H. Qamar, G. J. Nathan, Z. T. Alwahabi, K. D. King, in: Proc. Combust. Inst., volume 30, pp. 1493–1500.

[9] R. M. Frinstrom, A. A. Westenberg, Flame Structure, McGraw Hill, Inc., 1965.

[10] B. S. Haynes, H. G. Wagner, Prog. Energy Combust. Sci. 7 (1981) 229–273.

[11] R. S. Barlow, Proc. Combust. Inst. 31 (2007) 49–75.

[12] P. R. Medwell, P. A. M. Kalt, B. B. Dally, Combust. Flame 152 (2008) 100–113.

[13] K. Kohse-Höinghaus, J. B. Jeffries, Applied Combustion Diagnostics, Taylor & Francis, 2002.

[14] A. T. Hartlieb, B. Atakan, K. Kohse-Höinghaus, Appl. Phys. B 70 (2000) 435–445.

[15] D. Hofmann, A. Leipertz, Proc. Combust. Inst. 26 (1996) 945–950.

[16] S. P. Kearney, R. W. Schefer, S. J. Beresh, T. W. Grasser, Appl. Opt. 44 (2005) 1548–1558.

[17] W. Stricker, R. Lückerath, U. Meier, W. Meier, J. Raman Spectrosc. 34 (2003) 922–931.

[18] M. C. Weikl, T. Seeger, M. Wendler, R. Sommer, F. Beyrau, A. Leipertz, Proc. Combust. Inst. 32 (2009) 745–752.

[19] D. Most, A. Leipertz, Appl. Opt. 40 (2001) 5379–5387.

[20] G. A. Robinson, R. P. Lucht, N. M. Laurendeau, Appl. Opt 47 (2008) 2852–2858.

[21] D. Dabiri, Exp. Fluids 46 (2009) 191–241.

[22] G. Särner, M. Richter, M. Aldén, Opt. Lett. 33 (2008) 1327–1329.

[23] J. E. Dec, J. O. Keller, Proc. Combust. Inst. 21 (1986) 1737–1745.

[24] C. F. Kaminski, J. Engström, M. Aldén, Proc. Combust. Inst. 27 (1998) 85–93.

[25] H. Haraguchi, B. Smith, S. Weeks, D. J. Johnson, J. D. Winefordner, Appl. Spectrosc. 31 (1977) 156–163.

[26] J. Engström, J. Nygren, M. Aldén, C. F. Kaminski, Opt. Lett. 25 (2000) 1469–1471.

[27] J. Nygren, J. Engström, J. Walewski, C. F. Kaminski, M. Aldén, Meas. Sci. Technol. 12 (2001) 1294–1303.

[28] R. G. Joklik, J. W. Daily, Appl. Opt. 21 (1982) 4158–4162.

[29] P. R. Medwell, Q. N. Chan, P. A. M. Kalt, Z. T. Alwahabi, B. B. Dally, G. J. Nathan, Appl. Opt. 48 (2009) 1237–1248.

[30] C. Schulz, B. F. Kock, M. Hofmann, H. Michelsen, S. Will, B. Bougie, R. Suntz, G. Smallwood, Appl. Phys. B 83 (2006) 333–354.

[31] P. R. Medwell, Q. N. Chan, P. A. M. Kalt, Z. T. Alwahabi, B. B. Dally, G. J. Nathan, Appl. Spectrosc. 64(2) (2010) 173–176.

[32] J. H. Kent, S. J. Bastin, Combust. Flame 56 (1984) 29–42.

[33] N. H. Qamar, Z. T. Alwahabi, Q. N. Chan, G. J. Nathan, D. Roekaerts, K. D. King, Combust. Flame 156 (2009) 1339–1347.

[34] R. L. Vander Wal, Appl. Opt. 35 (1996) 6548–6559.

[35] J. Zerbs, K. P. Geigle, O. Lammel, J. Hader, R. Stirn, R. Hadef, W. Meier, Appl. Phys. B 96 (2009) 683–694.

[36] T. C. Williams, C. R. Shaddix, K. A. Jensen, J. M. Auo-Antilla, Int. J. Heat Mass Transfer 50 (2007) 1616–1630.

[37] K. C. Smyth, C. R. Shaddix, Combust. Flame 107 (1996) 314–320.

[38] J. Zhu, M. Y. Choi, G. W. Mulholland, S. L. Manzello, L. A. Gritzo, J. Suo-Anttilla, Proc. Combust. Inst. 29 (2002) 2367–2374.

[39] H. Bladh, J. Johnsson, P. E. Bengtsson, Appl. Phys. B 90 (2008) 109–125.

[40] J. Reimann, S. A. Suhlmann, S. Will, Combust. Flame 153 (2008) 650–654.

[41] A. V. Menon, S. Y. Lee, M. J. Linevsky, T. A. Litzinger, R. J. Santoro, Proc. Combust. Inst. 31 (2007) 593–601.

[42] L. M. Pickett, J. B. Ghandhi, Combust. Flame 132 (2003) 138–156.

[43] M. P. Lee, B. K. McMillin, R. K. Hanson, Appl. Opt. 32 (1993) 5379–5396.

[44] B. K. McMillin, J. L. Palmer, R. K. Hanson, Appl. Opt. 32(36) (1993) 7532–7545.

List of Figures

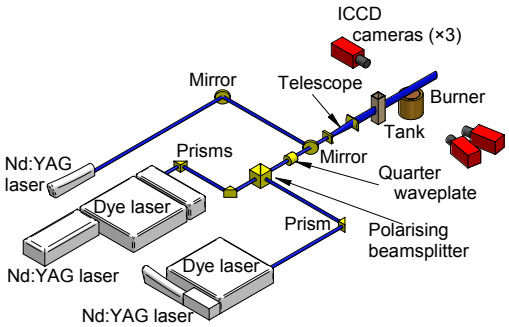

Figure 1: (Colour online) Schematic diagram of experimental layout.

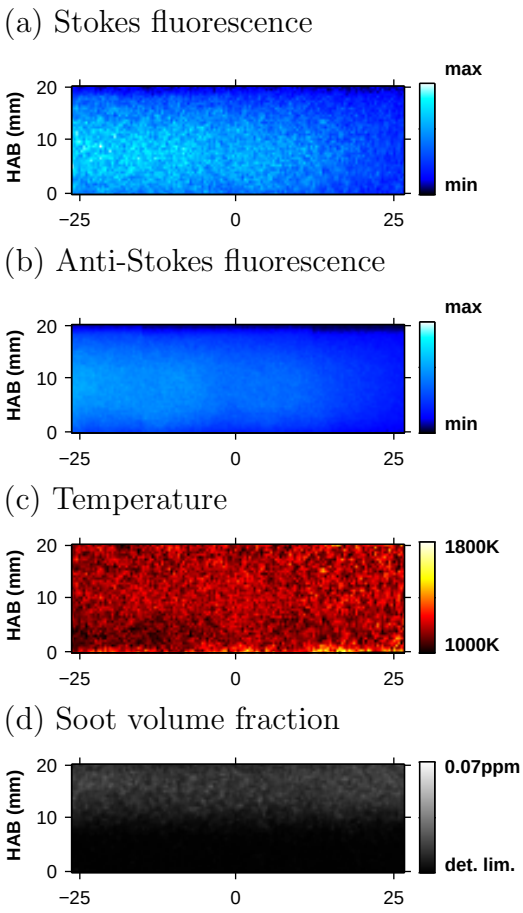

Figure 2: (Colour online) Simultaneous single-shot images for a laminar premixed ethylene-air flame. (a) Stokes, (b) anti-Stokes indium fluorescence, (c) NTLAF temperature, and (d) LII soot volume fraction. Image size approximately 20 mm×50 mm. Laser propagation from left to right.

(a) Stokes fluorescence

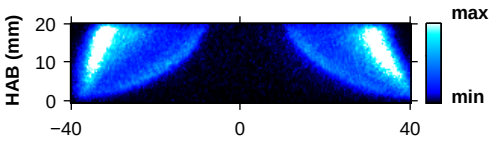

(b) Anti-Stokes fluorescence

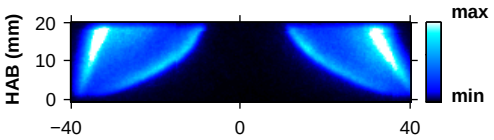

(c) Temperature

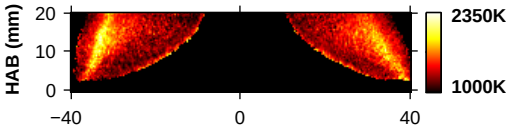

(d) Soot volume fraction

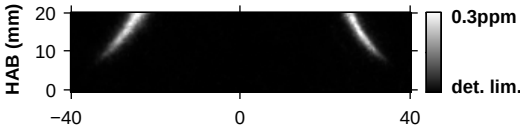

(e) Temperature and soot volume fraction

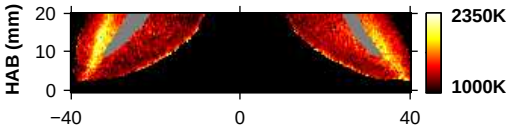

Figure 3: (Colour online) Simultaneous single-shot images for a laminar nonpremixed ethylene-air flame. (a) Stokes, (b) anti-Stokes indium fluorescence, (c) NTLAF temperature, (d) LII soot volume fraction, and (e) instantaneous temperature field with location of soot overlaid (in grey). Image size approximately 20 mm×80 mm. Laser propagation from left to right.

(a) Stokes fluorescence

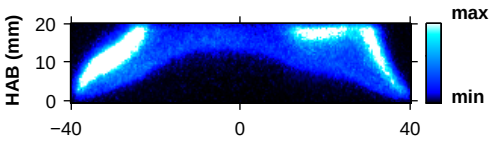

(b) Anti-Stokes fluorescence

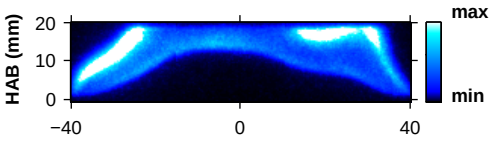

(c) Temperature

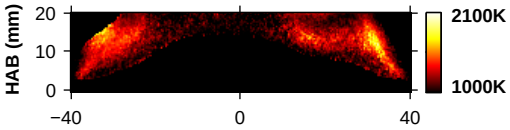

(d) Soot volume fraction

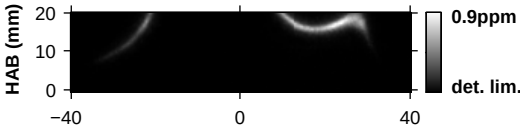

(e) Temperature and soot volume fraction

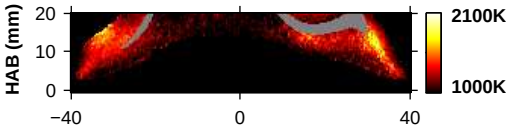

Figure 4: (Colour online) Simultaneous single-shot images of a wrinkled nonpremixed ethylene-air flame. (a) Stokes, (b) anti-Stokes indium fluorescence, (c) NTLAF temperature, (d) LII soot volume fraction, and (e) instantaneous temperature field with location of soot overlaid (in grey). Image size approximately 20 mm×80 mm. Laser propagation from left to right.

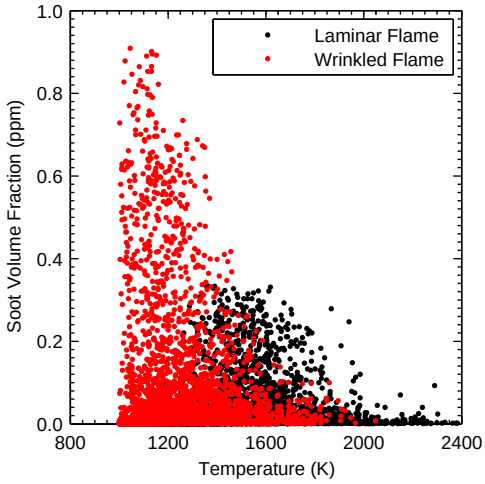

Figure 5: (Colour online) Soot volume fraction as a function of temperature for laminar nonpremixed and wrinkled nonpremixed flames.